



Automated tuning of a ring-assisted MZI-based interleaver for Kerr frequency combs

SONGLI WANG,¹ YUYANG WANG,¹ SWARNAVA SANYAL,² ROBERT PARSONS,¹ XINGCHEN JI,¹ YOSHITOMO OKAWACHI,² XIANG MENG,¹ MICHAL LIPSON,^{1,2} ALEXANDER GAETA,^{1,2} AND KEREN BERGMAN^{1,*}

¹Department of Electrical Engineering, Columbia University, New York, New York 10027, USA

²Department of Applied Physics and Applied Mathematics, Columbia University, New York, New York 10027, USA

*bergman@ee.columbia.edu

Received 4 November 2024; revised 19 December 2024; accepted 19 December 2024; posted 20 December 2024; published 15 January 2025

We demonstrate a compact ring-assisted Mach-Zehnder interferometer (RAMZI)-based silicon photonic interleaver with a 400 GHz free spectral range (FSR), featuring flat passbands exceeding a spectral range of 50 nm. Additionally, we introduce a novel, to the best of our knowledge, add-on structure and tuning method enabling automated compensation for fabrication imperfections, precise shaping of the RAMZI flat-top passbands, and alignment with Kerr comb lines. Experimental results have shown successful interleaving of eight channels of distributed-feedback (DFB) lasers as well as a 200 GHz Kerr comb, both achieving an extinction ratio of approximately 20 dB. © 2025 Optica Publishing Group. All rights, including for text and data mining (TDM), Artificial Intelligence (AI) training, and similar technologies, are reserved.

<https://doi.org/10.1364/OL.546772>

With the rapid growth of AI technology and the escalating demand for computing resources, there is an increasing need for faster and more cost-effective optical interconnects. The synergy between silicon photonics (SiPh) and dense wavelength-division multiplexing (DWDM) technology has paved the way for link architectures to achieve ultrahigh bandwidth densities and ultra-low energy consumption per bit. It has proven to be a viable solution to alleviate system-wide bandwidth bottlenecks [1,2]. Microresonator-based Kerr frequency combs provide a pathway to energy-efficient DWDM architectures [3,4]. In such comb-driven DWDM systems, interleavers are key building blocks that help multiplex and demultiplex adjacent wavelength channels. They become particularly crucial in multi-FSR systems [5] by effectively doubling the channel spacing, thus significantly reducing the inter-channel cross talk and enhancing the bandwidth utilization. The simplest realization of an interleaver is an unbalanced Mach-Zehnder interferometer (MZI). While MZI-based interleavers are compact and straightforward to design, the sinusoidal response is far from the ideal square-wave response, which results in a high sensitivity to perturbations and also a limited channel capacity due to fundamental dispersion. For this reason, several solutions have been proposed to achieve a flat-top response, e.g., ring-assisted Mach-Zehnder interferometers (RAMZIs) and MZI lattice filters. RAMZI-based

interleavers incorporate ring resonators on MZI arms to achieve flat-top passbands [6–8]. This feature enhances its resilience to both perturbations and the FSR mismatch w.r.t. the DWDM source while maintaining a compact footprint. However, the flat-top response comes with the complexity of additional rings and phase shifters, requiring a more intricate control scheme. The automated control for MZI-based interleavers and MZI lattice-based interleavers has been proposed and demonstrated in [9], but there lacks an effective method for controlling RAMZI-based interleavers to the best of our knowledge.

In our prior work [10,11], we proposed a RAMZI auto-tuning structure and validated its efficacy to align the RAMZI interleaver with an eight-channel DFB laser array. In this Letter, we present the first demonstration of an interleaved Kerr comb achieved by a RAMZI interleaver with automated control. This innovative solution is designed to automatically compensate for phase errors between the ring and the MZI delay arm and offer robust alignment with the frequency comb source while still maintaining a compact overall structure.

The schematic of a single-ring RAMZI is shown in Fig. 1(a). Besides two 3 dB couplers and asymmetric arms with ΔL length difference, RAMZI consists of an additional ring resonator with a circumference of L_r on the shorter arm. Leveraging the rapid phase change across the resonance of the ring resonator [12], RAMZI can exhibit a steep roll-off and flat-top response. To understand the formation of the flat-top response, the steady-state response of the ring resonator can be broken down into multiple independent paths with integer times of the ring circumference, as explained in [13]. The critical RAMZI length relation between ΔL and L_r is found to be $\beta L_r = 2\beta\Delta L \pm \pi$, where $\beta = 2\pi n_{eff}/\lambda_0$ is the phase constant. Denoting the phase term as $\Phi = \beta L_r/2$, the transmission of a single-ring RAMZI can be obtained in Fourier series as follows:

$$T = \frac{1}{2} + \frac{1}{2} \left[\tau \sin \Phi + \sum_{n=1}^{\infty} \kappa^2 \tau^{n-1} \sin(2n-1)\Phi \right], \quad (1)$$

where κ and τ are the cross- and self-coupling coefficients of the ring resonator, respectively. The ring coupling coefficients can be optimized by comparing the Fourier coefficients between

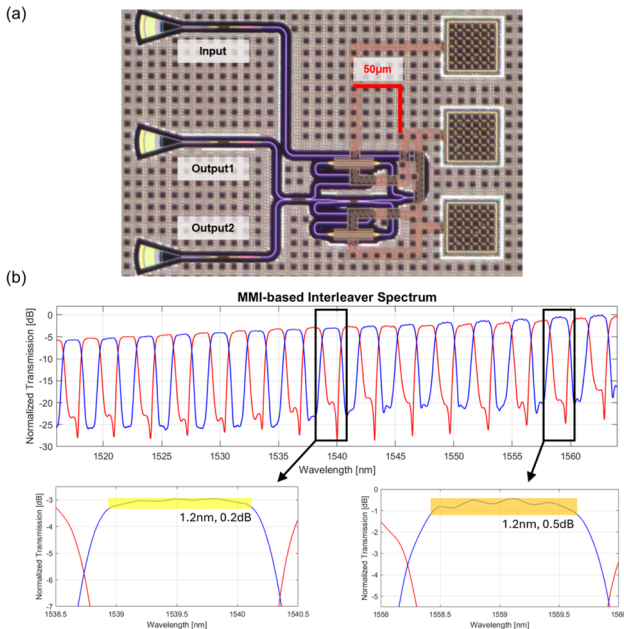


Fig. 1. (a) Fabricated 400 GHz MMI coupler-based RAMZI interleaver. (b) Measured 400 GHz RAMZI interleaver spectrum, including a zoomed-in view of passbands. The red and blue curves represent each of the two interleaver output ports.

RAMZI transmission and the square wave. In this way, the optimal κ is found to be around 0.92, corresponding to an 85% power splitting ratio.

Compared with directional couplers, multi-mode interferometer (MMI) couplers exhibit a broader operational bandwidth, which is particularly beneficial in applications with Kerr combs, as the comb source can generate a great number of comb lines spanning more than a hundred nanometers. However, MMI couplers are usually unavailable with special power splitting ratios other than 50:50. In order to achieve a broadband performance while reaching the target power splitting ratio, we designed a compact low-loss MMI coupler with a “bow-tie” shape, meaning the MMI coupler width linearly changes from sides to the center, as shown in Fig. 2(b). We chose the original MMI width as 2 μm, and the center width was optimized to be 2.02 μm. The footprint of the MMI coupler is 2.02 μm × 19.2 μm including the taper waveguides. The FDTD simulation results are shown in Fig. 2(c), and the simulated excess loss is 0.05 dB.

The fabricated RAMZI with a 400 GHz FSR, designed for de-interleaving a 200 GHz-spacing DWDM source, is illustrated in Fig. 1(a). Two thermal phase shifters are placed on the longer MZI arm and inside the ring, respectively, with a high thermal tuning efficiency of 20 mW/π. To analyze the RAMZI transmission spectrum, a tunable laser (Keysight N7778C) sends light across 1516–1564 nm with a 10 pm resolution into the photonic integrated circuit (PIC), and the transmission is measured by an optical power meter (Keysight N7742C), which is plotted in Fig. 1(b). The transmission spectrum exhibits a flat-top response after applying 1 V to the phase shifter on the MZI arm, with an extinction ratio of 20 dB over 50 nm bandwidth for both ports. Note that the unevenness in the envelope of the spectrum is primarily introduced by the grating coupler rather than by the RAMZI. The zoomed-in view of RAMZI passbands is shown in Fig. 1(b). Around 1540 nm, the passband shows <0.2 dB fluctuation over a 1.2 nm bandwidth, while at around 1559 nm, it

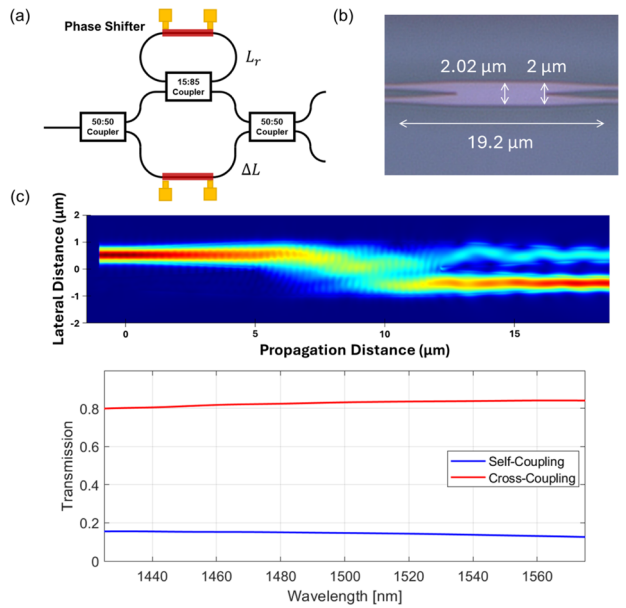


Fig. 2. (a) Schematic of the general single-ring RAMZI interleaver. (b) Fabricated “bow-tie” MMI coupler with 15:85 splitting ratio. (c) FDTD simulation results of the MMI coupler. The red and blue curves represent cross- and self-power coupling ratios, respectively.

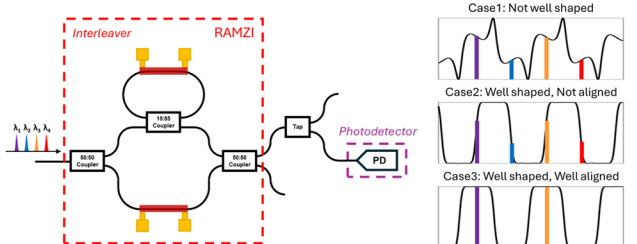


Fig. 3. Schematic of the RAMZI interleaver directly connecting a PD for power monitoring. Assuming equal comb line powers and equal PD responsivity, the PD will generate a constant current in all three cases.

exhibits <0.5 dB fluctuation over the same bandwidth. This degradation is attributed in part to the grating coupler and in part to the variations in the power splitting ratio of the MMI coupler at higher wavelengths, as illustrated in Fig. 2(c).

To ensure automatic compensation of phase errors and automatic alignment of the interleaver passbands to the DWDM channels, a photodetector is necessary for generating a feedback signal, as seen in various auto-tuning architectures [14–16]. However, directly tapping MZI output ports for photocurrent monitoring cannot generate enough feedback, as analyzed in [9]. Assuming the DWDM source has the same power among all the wavelength channels, either MZI port will always output a constant optical power, rendering it unusable for auto-tuning. This issue remains for RAMZI structures, as shown in Fig. 3. Each RAMZI port always passes through half of the total DWDM source power, no matter if the RAMZI is tuned well for flat-top transmission or aligned well with the DWDM source.

We have devised an auto-tuning structure for our RAMZI interleaver, as depicted in Fig. 4(a). The RAMZI (red box) functions as the link (de)interleaver, with a power tap integrated

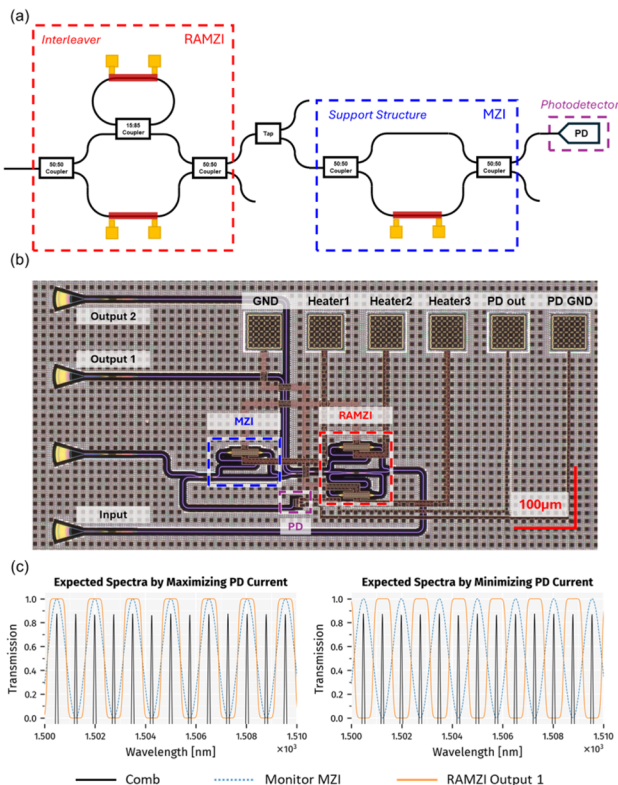


Fig. 4. (a) Schematic of the proposed auto-tuning structure: adding an MZI with the same FSR as the control support structure (blue box) to the RAMZI interleaver (red box), followed by a PD as the monitor. (b) Fabricated RAMZI interleaver with the auto-tuning structure. (c) Simulation results of the optimized spectra by maximizing/minimizing PD current.

into its output to divert a small portion of optical power for auto-control feedback, while most power continues to subsequent devices. The supporting control structure (blue box) is composed of an MZI with an identical FSR to that of the RAMZI, followed by a photodetector. With this additional MZI, the output photocurrent is no longer constant. Specifically, the current will reach its maximum when the passbands of both the RAMZI and MZI are aligned with the DWDM signals, and will be minimized when their passbands offset with one another by a single channel spacing, as illustrated in Fig. 4(b). Therefore, the RAMZI transmission spectrum can be optimized for both flat-top shape and channel alignment by either maximizing or minimizing the photocurrent.

The fabricated RAMZI auto-tuning structure is shown in Fig. 4(c), which involves three heaters: one in the supporting MZI (Heater 1), one in the MZI arm of the RAMZI (Heater 2), and the last in the ring of the RAMZI (Heater 3). The optimization procedure is carried out in the following sequential steps:

1. **repeat** adjusting Heater i **until** max/min PD reading;
2. **repeat** adjusting Heater 2 and Heater 3 with equal voltage increments **until** max/min PD reading;
3. **repeat** adjusting Heater 2 and Heater 3 with opposite voltage increments **until** max/min PD reading;
4. **repeat** steps 1 to 3 **until** no improvement in PD reading;

Algorithm 1. Single heater tuning procedure

```

Input: Voltage of Heater  $i$  –  $V_i$ 
Feedback: Photocurrent –  $I$ , Best photocurrent value –  $I_{opt}$ 
 $V_i \leftarrow V_{i0}$                                 ▷ Set initial voltages and read current
 $I_{opt} \leftarrow I_0$ 
for  $i = 1 : 3$  do                         ▷ Optimize three heaters one by one
     $V_i \leftarrow V_i + \Delta V_i$                 ▷ Try increasing heater voltage first
    if  $I > I_{opt}$  then
         $I_{opt} \leftarrow I$ 
    repeat                                     ▷ Keep going if current increases
         $V_i \leftarrow V_i + \Delta V_i$ 
         $I_{opt} \leftarrow I$ 
    until  $I \leq I_{opt}$                          ▷ Stop with maximized current
    else
         $V_i \leftarrow V_i - \Delta V_i$                 ▷ Reduce heater voltage
        if  $I > I_{opt}$  then
             $I_{opt} \leftarrow I$ 
        repeat                                     ▷ Keep going if current increases
             $V_i \leftarrow V_i - \Delta V_i$ 
             $I_{opt} \leftarrow I$ 
        until  $I \leq I_{opt}$                          ▷ Stop with maximized current

```

where the adjustment to heater power at each step is performed in a binary search manner as described in [9]. As an example, the single heater tuning process for maximizing photocurrent, i.e., step 1, is shown in Algorithm 1. Steps 2 and 3 are similar to step 1 except that two heaters need to be adjusted simultaneously. Note that adjustments to voltage increments may be needed, as larger voltage increments help to avoid local optima, while smaller voltage increments help to fine-tune to the global optimum.

The experimental setup for validating the interleaver auto-tuning is depicted in Fig. 5(a). The setup consists of eight DFB lasers with a 200 GHz channel spacing. The DWDM channels are directed into the interleaver chip combined with a broadband light source. The output light from the interleaver is sent to a

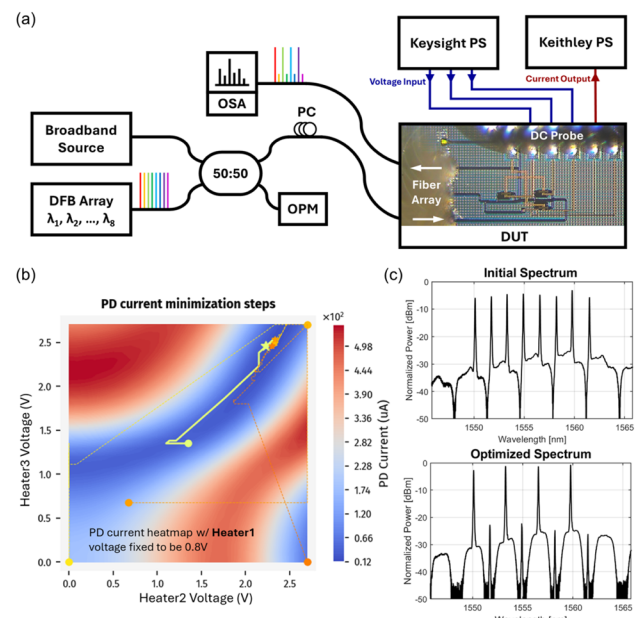


Fig. 5. (a) Experimental setup of the RAMZI interleaver auto-tuning test. (b) PD current heatmap and optimization paths plotted for a Heater 1 voltage of 0.8 V, which is also the optimal Heater 1 voltage found. (c) RAMZI interleaver spectra with DWDM source before and after the auto-tuning.

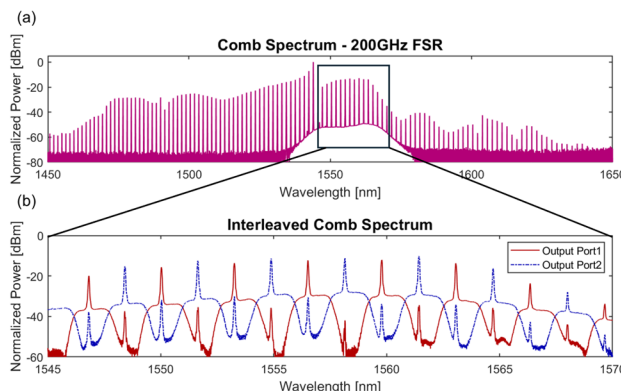


Fig. 6. (a) Spectrum of the 200 GHz Kerr comb. (b) Spectra of the interleaved Kerr comb from two output ports of the RAMZI interleaver. The interleaver spectra are demonstrated by combining a broadband light source with the Kerr comb.

Yokogawa optical spectrum analyzer (OSA), realizing real-time spectrum inspection during the optimization process. Note that the broadband source and the OSA serve only for visualization purposes and are not essential to the auto-tuning process. The power of the broadband source is controlled to be much less than the DWDM source to ensure that it does not impact the auto-tuning process. For interleaver thermal control, a DC probe is landed on the six pads, linking the interleaver structure to the power supplies. A Keysight multichannel power supply delivers voltages for the three heaters, acting as the optimization inputs, while a Keithley high-precision power supply provides bias voltage to the photodetector, reading the output photocurrent as the optimization output. Figure 5(c) shows the PD current heatmap along with the optimization paths. Dots of various colors represent the attempted initial voltages and stars represent the final voltages after the auto-tuning process, all of which converge to the optimal point with minor differences caused by the precision of the measuring equipment. Figure 5(b) displays the initial and final interleaver spectra corresponding to the highlighted yellow path in Fig. 5(c), demonstrating the optimized interleaver extinction ratio over 20 dB and the precise alignment of the passbands with the DWDM source. The time required for the auto-tuning process varies with the initial phase errors of each component. In our experiment, we vary the initial conditions and observe that the tuning converges within an average of 200 steps. This process is expected to be completed within 4 ms assuming an application-specific integrated circuit (ASIC) controlling the PIC. This estimate assumes that the time for each tuning step is dominated by the heater time constant of 20 μ s.

Finally, we demonstrate the interleaving of a normal-group velocity dispersion (GVD) Kerr comb with a 200 GHz channel spacing, the spectrum of which is shown in Fig. 6(a). We sent the comb source into the 400 GHz RAMZI auto-tuning structure combined with the broadband source as before, and the interleaved comb spectra are shown in Fig. 6(b). Due to the bandwidth limitation of the grating couplers, the demonstrated interleaved comb spectra only covers 1545–1570 nm, but it shows that the

RAMZI interleaver was well tuned, exhibiting a flat-top response and an extinction ratio of around 20 dB, confirming the effectiveness and robustness of this auto-tuning structure and control scheme. For the RAMZI design, we think the splitting ratio of the fabricated MMI deviates slightly from the target as this is the first design iteration. The performance of the RAMZI in terms of extinction ratio and passband flatness is expected to improve with further refinement of the coupler design.

In summary, we presented a novel RAMZI auto-tuning structure and control scheme. The proposed auto-tuning structure effectively compensates for phase errors and optimizes passband alignment with DWDM channels, promoting operational efficiency and performance enhancement. This development can drive the ongoing evolution of DWDM link architectures in high-performance computing systems and data centers, fostering the realization of more efficient and scalable communication infrastructures.

Funding. Defense Advanced Research Projects Agency (HR00111 830002, HR00111920014); Advanced Research Projects Agency - Energy (DE-AR000843); Center for Ubiquitous Connectivity, (CubiC) sponsored by the Semiconductor Research Corporation (SRC) and DARPA under the JUMP 2.0 program.

Acknowledgments. The authors wish to thank Abhinav Vinod, Kaveh Hosseini, and Tim Tri Hoang from Intel Corporation for technical discussion.

Disclosures. The authors declare no conflicts of interest.

Data availability. Data underlying the results presented in this Letter are not publicly available at this time but may be obtained from the authors upon reasonable request.

REFERENCES

- Y. Wang, A. Novick, R. Parsons, *et al.*, *Proc. SPIE* **12429**, 124291F (2023).
- S. Daudlin, A. Rizzo, S. Lee, *et al.*, “3D photonics for ultra-low energy, high bandwidth-density chip data links,” *arXiv* (2023).
- B. Y. Kim, Y. Okawachi, J. K. Jang, *et al.*, *Opt. Lett.* **44**, 4475 (2019).
- A. Rizzo, A. Novick, V. Gopal, *et al.*, *Nat. Photonics* **17**, 781 (2023).
- A. James, A. Novick, A. Rizzo, *et al.*, *Optica* **10**, 832 (2023).
- L.-W. Luo, S. Ibrahim, A. Nitkowski, *et al.*, *Opt. Express* **18**, 23079 (2010).
- J. Song, Q. Fang, S. Tao, *et al.*, *Opt. Express* **16**, 8359 (2008).
- A. Singh, R. Belansky, and M. Soltani, *Opt. Express* **30**, 43787 (2022).
- T. Akiyama, S. Oda, Y. Nakasha, *et al.*, *Opt. Express* **29**, 7966 (2021).
- S. Wang, Y. Wang, X. Meng, *et al.*, in *Optical Fiber Communication Conference* (Optica Publishing Group, 2024), paper Th1A-3.
- Y. Wang, S. Wang, R. Parsons, *et al.*, *IEEE Transactions on Components, Packaging and Manufacturing Technology* (2024), p. 1.
- W. Bogaerts, P. De Heyn, T. Van Vaerenbergh, *et al.*, *Laser Photonics Rev.* **6**, 47 (2012).
- Z.-C. Huang, X. Meng, and R. Osgood, in *2020 Conference on Lasers and Electro-Optics (CLEO)* (IEEE, 2020), pp. 1–2.
- H. Matsuura, K. Suzuki, S. Suda, *et al.*, in *Optical Fiber Communication Conference* (Optica Publishing Group, 2018), paper M4H-2.
- M. AlTaha, H. Jayatilleka, Z. Lu, *et al.*, *Opt. Express* **27**, 24747 (2019).
- K. Entesari, S. Palermo, C. Madsen, *et al.*, in *Optical Fiber Communication Conference* (Optica Publishing Group, 2022), paper Th1D-6.